Propagation model for vector beams generated by metasurfaces

Weixing Shu,[1,4] Yachao Liu,[2] Yougang Ke,[2] Xiaohui Ling,[2] Zhenxing Liu,[2] Bin Huang,[2] Hailu Luo,[2,5] and Xiaobo Yin[3,6]

[1]*Key Laboratory for Micro-Nano-Optoelectronic Devices of Ministry of Education, College of Computer Science and Electronic Engineering, Hunan University, Changsha 410082, China*

[2]*Laboratory for Spin Photonics, School of Physics and Electronics, Hunan University, Changsha 410082, China*

[3]*Department of Mechanical Engineering, University of Colorado, Boulder, CO 80309, USA*

[4]*wxshu@hnu.edu.cn*

[5]*hailuluo@hnu.edu.cn*

[6]*xiaobo.yin@colorado.edu*

Abstract: A propagation model of vector beams generated by metasurfaces based on vector diffraction theory is established theoretically and verified experimentally. Considering the Pancharatnam-Berry phase introduced by the metasurface, analytical forms of vector beams for arbitrary incident polarization and topological charge of metasurfaces are found in the Fresnel and Fraunhofer diffraction regions, respectively. The complex amplitude of the resultant vector beam can be described in terms of a confluent hypergeometric function, with an intensity profile that manifests concentric rings in the Fresnel region and a single ring in the Fraunhofer one. Fraunhofer diffraction provides a method to create vector beams with simultaneously high purity and modal power. Further experiments verify the theoretical results.

References and links

1. For a review, see Q. Zhan, "Cylindrical vector beams: from mathematical concepts to applications," Adv. Opt. Photon. **1**(1), 1–57 (2009) and references therein.
2. A. Holleczek, A. Aiello, C. Gabriel, C. Marquardt, and G. Leuchs,"Classical and quantum properties of cylindrically polarized states of light," Opt. Express **19**(10), 9714–9736 (2011).
3. G. Milione, H. I. Sztul, D. A. Nolan, and R. R. Alfano, "Higher-order Poincaré sphere, Stokes parameters, and the angular momentum of light," Phys. Rev. Lett. **107**(5), 053601 (2011).
4. C. Hnatovsky, V. G. Shvedov, W. Krolikowski, and A. V. Rode, "Materials processing with a tightly focused femtosecond laser vortex pulse," Opt. Lett. **35**(20), 3417–3419 (2010).
5. W. Kimura, G. H. Kim, R. D. Romea, L. C. Steinhauer, I. V. Pogorelsky, K. P. Kusche, R. C. Fernow, X. Wang, and Y. Liu, "Laser acceleration of relativistic electrons using the inverse Cherenkov effect," Phys. Rev. Lett. **74**(4), 546–549 (1995).
6. B. J. Roxworthy and K. C. Toussaint Jr., "Optical trapping with π-phase cylindrical vector beams," New J. Phys. **12**(7), 073012 (2010).
7. A. F. Abouraddy and K. C. Toussaint Jr., "Three-dimensional polarization control in microscopy," Phys. Rev. Lett. **96**(15), 153901 (2006).
8. L. Novotny, M. R. Beversluis, K. S. Youngworth, and T. G. Brown, "Longitudinal field modes probed by single molecules," Phys. Rev. Lett. **86**(23), 5251-5254 (2001).
9. V. D'Ambrosio, N. Spagnolo, L. D. Re, S. Slussarenko, Y. Li, L. C. Kwek, L. Marrucci, S. P. Walborn, L. Aolita, and F. Sciarrino, "Photonic polarization gears for ultra-sensitive angular measurements," Nat. Commun. **4**, 2432 (2013).
10. G. Milione, M. P. J. Lavery, H. Huang, Y. Ren, G. Xie, T. A. Nguyen, E. Karimi, L. Marrucci, D. A. Nolan, R. R. Alfano, and A. E. Willner, "4 × 20 Gbit/s mode division multiplexing over free space using vector modes and a q-plate mode (de)multiplexer," Opt. Lett. **40**(9), 1980–1983 (2015).
11. G. Milione, T. A. Nguyen, J. Leach, D. A. Nolan, and R. R. Alfano, "Using the nonseparability of vector beams to encode information for optical communication," Opt. Lett. **40**(21), 4887–4890 (2015).
12. V. D'Ambrosio, E. Nagali, S. P. Walborn, L. Aolita, S. Slussarenko, L. Marrucci, and F. Sciarrino, "Complete experimental toolbox for alignment-free quantum communication," Nat. Commun. **3**, 961 (2012).

13. C. Maurer, A. Jesacher, S. Fürhapter, S. Bernet, and M. Ritsch-Marte, "Tailoring of arbitrary optical vector beams," New J. Phys. **9**(3), 78 (2007).
14. A. M. Beckley, T. G. Brown, and M. A. Alonso, "Full Poincaré beams," Opt. Express **18**(10), 10777–10785 (2010).
15. E. J. Galvez, S. Khadka, W. H. Schubert, and S. Nomoto, "Poincaré-beam patterns produced by nonseparable superpositions of Laguerre-Gauss and polarization modes of light," Appl. Opt. **51**(15), 2925–2934 (2012).
16. D. Maluenda, I. Juvells, R.Martínez-Herrero, and A. Carnicer, "Reconfigurable beams with arbitrary polarization and shape distributions at a given plane," Opt. Express **21**(5), 5424–5431 (2013).
17. X. L. Wang, J. P. Ding, W. J. Ni, C. S. Guo, and H. T. Wang, "Generation of arbitrary vector beams with a spatial light modulator and a common path interferometric arrangement," Opt. Lett. **32**(24), 3549–3551 (2007).
18. Z. Bomzon, G. Biener, V. Kleiner, and E. Hasman, "Radially and azimuthally polarized beams generated by space-variant dielectric subwavelength gratings," Opt. Lett. **27**(5), 285–287 (2002).
19. E. Hasman, G. Biener, A. Niv, and V. Kleiner, "Space-variant polarization manipulation," Prog. Opt. **47** 215–289 (2005).
20. L. Marrucci, C. Manzo, and D. Paparo, "Optical spin-to-orbital angular momentum conversion in inhomogeneous anisotropic media," Phys. Rev. Lett. **96**(16), 163905 (2006).
21. A. Niv, G. Biener, V. Kleiner, and E. Hasman, "Manipulation of the Pancharatnam phase in vectorial vortices," Opt. Express **14**(10), 4208–4220 (2006).
22. R. Dorn, S. Quabis, and G. Leuchs, "Sharper focus for a radially polarized light beam," Phys. Rev. Lett. **91**(23), 233901 (2003).
23. G. Machavariani, Y. Lumer, I. Moshe, A. Meir, and S. Jackel, "Efficient extracavity generation of radially and azimuthally polarized beams," Opt. Lett. **32**(11), 1468–1470 (2007).
24. G. Milione, A. Dudley, T. A. Nguyen, O. Chakraborty, E. Karimi, and A. Forbes, "Measuring the self-healing of the spatially inhomogeneous states of polarization of vector Bessel beams," J. Opt. **17**(3), 035617 (2015).
25. M. Beresna, M. Gecevičius, P. G. Kazansky, and T. Gertus, "Radially polarized optical vortex converter created by femtosecond laser nanostructuring of glass," Appl. Phys. Lett. **98**(20), 201101 (2011).
26. M. Beresna, M. Gecevičius, and P. G. Kazansky, "Polarization sensitive elements fabricated by femtosecond laser nanostructuring of glass," Opt. Mat. Express **1**(4), 783–795 (2011).
27. F. Cardano, E. Karimi, S. Slussarenko, L. Marrucci, C. de Lisio, and E. Santamato, "Polarization pattern of vector vortex beams generated by q-plates with different topological charges," Appl. Opt. **51**(10), C1-C6 (2012).
28. V. D'Ambrosio, F. Baccari, S. Slussarenko, L. Marrucci, and F. Sciarrino, "Arbitrary, direct and deterministic manipulation of vector beams via electrically-tuned q-plates," Sci. Report **5**, 7840 (2015).
29. Y. Liu, X. Ling, X. Yi, X. Zhou, H. Luo, and S. Wen, "Realization of polarization evolution on higher-order Poincaré sphere with metasurface," Appl. Phys. Lett. **104**(19), 191110 (2014).
30. P. Chen, W. Ji, B.-Y. Wei, W. Hu, V. Chigrinov, and Y.-Q. Lu, "Generation of arbitrary vector beams with liquid crystal polarization converters and vector-photoaligned q-plates," Appl. Phys. Lett. **107**(24), 241102 (2015).
31. D. Naidoo, F. S. Roux, A. Dudley, I. Litvin, B. Piccirillo, L. Marrucci, and A. Forbes, "Controlled generation of higher-order Poincaré sphere beams from a laser," Nat. Photonics **10**(5), 327–332 (2016).
32. E. Karimi, S. Slussarenko, B. Piccirillo, L. Marrucci, and E. Santamato, "Polarization-controlled evolution of light transverse modes and associated Pancharatnam geometric phase in orbital angular momentum," Phys. Rev. A **81**(5), 053813 (2010).
33. S. Slussarenko, A. Murauski, T. Du, V. Chigrinov, L. Marrucci, and E. Santamato, "Tunable liquid crystal q-plates with arbitrary topological charge," Opt. Express **19**(5), 4085–4090 (2011).
34. G. F. Calvo and A. Picón, "Spin-induced angular momentum switching," Opt. Lett. **32**(7), 838–840 (2007).
35. E. Karimi, B. Piccirillo, L. Marrucci, and E. Santamato, "Light propagation in a birefringent plate with topological charge," Opt. Lett. **34**(8), 1225–1227 (2009).
36. X. Ling, X. Zhou, H. Luo, and S. Wen, "Steering far-field spin-dependent splitting of light by inhomogeneous anisotropic media," Phys. Rev. A **86**(5), 053824 (2012).
37. J. W. Goodman, *Introduction to Fourier Optics*, 3rd ed. (Roberts and Company Publishers, 2005).
38. A. Ciattoni, B. Crosignanic, and P. D. Porto, "Vectorial analytical description of propagation of a highly nonparaxial beam," Opt. Commun. **202**(1), 17–20 (2002).
39. M. Born and E. Wolf, *Principles of Optics* (Cambridge University Press, 1999).
40. B. E. A. Saleh and M. C. Teich, *Fundamentals of Photonics* (John Wiley and Sons, 2007).
41. W. Shu, Y. Ke, Y. Liu, X. Ling, H. Luo, and X. Yin, "Radial spin Hall effect of light," Phys. Rev. A **93**(1), 013839 (2016).
42. M. J. Stephen and J. P. Straley, "Physics of liquid crystals," Rev. Mod. Phys. **46**(4), 617–704 (1974).
43. M. Stalder and M. Schadt, "Linearly polarized light with axial symmetry generated by liquid-crystal polarization converters," Opt. Lett. **21**(23), 1948–1950 (1996).
44. J. A. Davis, N. Hashimoto, M. Kurihara, E. Hurtado, M. Pierce, M. M. Sánchez-López, K. Badham, and I. Moreno, "Analysis of a segmented q-plate tunable retarder for the generation of first-order vector beams," Appl. Opt. **54**(32), 9583–9590 (2015).
45. S. Pancharatnam, "Generalized theory of interference, and its applications," Proc. Indian Acad. Sci., Sect. A **44**(5), 247–262 (1956).
46. M. V. Berry, "The adiabatic phase and Pancharatnams phase for polarized light," J. Mod. Opt. **34**(11), 1401–1407

(1987).

47. I. S. Gradshteyn and I. M. Ryzhik, *Table of Integrals, Series, and Products*, 7th ed. (Academic Press, 2007).

48. M. Kang, J. Chen, B. Gu, Y. Li, L. T. Vuong, and H.-T. Wang "Spatial splitting of spin states in subwavelength metallic microstructures via partial conversion of spin-to-orbital angular momentum," Phys. Rev. A **85**(3), 035801 (2012).

49. G. Li, M. Kang, S. Chen, S. Zhang, E. Y. Pun, K. W. Cheah, and J. Li, "Spin-enabled plasmonic metasurfaces for manipulating orbital angular momentum of light," Nano Lett. **13**(9), 4148–4151 (2013).

50. X. Ling, X. Zhou, W. Shu, H. Luo, S. Wen, "Realization of tunable photonic spin hall effect by tailoring the Pancharatnam-Berry phase," Sci. Rep. **4**, 5557 (2014).

51. K. Y. Bliokh, F. J. Rodríguez-Fortuño, F. Nori, and A. V. Zayats "Spin-orbit interactions of light," Nat. Photonics **9**(12), 796–808 (2015).

52. G. Indebetouw, "Optical vortices and their propagation," J. Mod. Opt. **40**(1), 73–87 (1993).

53. Z. S. Sacks, D. Rozas, and G. A. Swartzlander, "Holographic formation of optical-vortex filaments," J. Opt. Soc. Am. B **15**(8), 2226–2234 (1998).

54. G. Peele and K. A. Nugent, "X-ray vortex beams: a theoretical analysis," Opt. Express **11**(19), 2315–2322 (2003).

55. V. V. Kotlyar, A. A. Almazov, S. N. Khonina, V. A. Soifer, H. Elfstrom, and J. Turunen, "Generation of phase singularity through diffracting a plane or Gaussian beam by a spiral phase plate," J. Opt. Soc. Am. A **22**(5), 849–861 (2005).

56. V. A. Pas'ko, I. V. Basistiy, M. V. Vasnetsov, and M. S. Soskin, "Analysis of optical vortex beams with integer and fractional topological charge," Proc. SPIE **5477**, 83–88 (2004).

57. A. Ya. Bekshaev and A. I. Karamoch, "Spatial characteristics of vortex light beams produced by diffraction gratings with embedded phase singularity," Opt. Commun. **281**(6), 1366–1374 (2008).

58. V. V. Kotlyar and A. A. Kovalev, "Family of hypergeometric laser beams," J. Opt. Soc. Am. A **25**(1), 262–270 (2008).

59. M. V. Berry, "Optical vortices evolving from helicoidal integer and fractional phase steps," J. Opt. A **6**(4), 259–268 (2004).

60. Z. J. Liu, H. F. Zhao, J. L. Liu, J. Lin, M. A. Ahmad, and S. T. Liu, "Generation of hollow Gaussian beams by spatial filtering," Opt. Lett. **32**(15), 2076–2078 (2007).

1. Introduction

In recent years much interest has been devoted to vector beams with polarization states that vary azimuthally in the beam cross section [1–3]. Due to these inhomogeneous polarization states, such vector beams have unique properties that lead to applications in material processing [4], particle acceleration [5], optical trapping [6], microscopy [7], precision metrology [8, 9], and classical and quantum communications [10–12], among others. Generation and manipulation of vector beams have been carried out using several methods [13–17]. Most recently researchers have constructed inhomogeneous anisotropic plates [18, 19], also named q-plates [20], to generate vector beams flexibly and efficiently [21–30].

Despite this success, vector beam generation by q-plates faces two challenges: theoretical description and mode purity. Firstly, the resultant vector fields are often analyzed based on the plane wave in the literature. While this simple model can conveniently account for associated qualitative effects, such as Pancharatnam-Berry (PB) phases [19–21] and vector polarization distributions [25–31], it cannot quantitatively describe the behavior of the propagating light beam. To take the beam dimensions into account, vector beams have often been simplified as Laguerre-Gaussian beams with vector polarizations in the literature [1–3, 13–15]. The effect of diffraction, though evidenced by experiments resulting in multi-ringed patterns of the vector beam [29–33], has been ignored. On this issue Calvo *et al.* firstly expressed the resultant beam as a Fresnel integral for an incident Laguerre-Gaussian beam [34]. Later, Karimi *et al.* used the zero-order asymptotic solution of Helmholtz's equation to calculate the Fresnel integral [35]. Importantly, they derived an analytical result which depends on the birefringence indices of the q-plate. In addition, Fraunhofer diffraction through a q-plate was numerically studied in [36]. Nevertheless, there is still not an explicit expression, independent of material parameters, for vector beams generated by q-plates, and corresponding experimental studies are also absent.

Secondly, as mentioned previously, diffraction leads vector beams generated by q-plates to contain many radial modes in which the energy of the central ring decreases dramatically with

increasing q. Therefore, it is difficult to simultaneously maximize purity and modal energy by this generation technique [31]. However, mode purity is crucial for the properties of vector beams and thus to their applications, especially those related to high precision [8, 9] and the quantum levels [12]. Most recently Naidoo *et al.* demonstrated an internal generation technique with q-plates inside a laser cavity that can create vector beams with high purity [31]. As for the commonly used technique with q-plates outside the laser cavity, however, generation of vector beams with high purity and maximized energy is still a challenge today.

In this article we focus on these issues. We present analytical models for vector beams produced by q-plates made from dielectric metasurfaces and then propose a method to create vector beams with all of the energy in a single mode. Following vector diffraction theory [37,38], a general form of the output beam from an arbitrary half-wave metasurface for arbitrary incident polarization is obtained for both the Fresnel and Fraunhofer diffraction regions. It is found that the resultant vector beam has a complex amplitude described by a hypergeometric function, and that its propagation is dependent on q and its position in space. The transverse intensity profile of the vector beam manifests itself as a set of concentric rings in the Fresnel diffraction region and a single ring in the Fraunhofer region. This latter result provides a method to obtain vector beams with simultaneously high purity and modal energies. Further experiments verify the theoretical results.

2. Theoretical formulation

In the most general case, a homogeneous elliptically polarized beam impinging on a wave plate at normal incidence is considered. The polarization can be geometrically represented by a point on the Poincaré sphere [39, 40] and algebraically described in terms of its polar angle ϑ and azimuthal angle φ on the sphere [15, 27]. Here the incident elliptical polarization is

$$\boldsymbol{E}_i(x, y, 0) = E_0(x, y)(\cos \vartheta e^{-i\varphi} |+\rangle + \sin \vartheta e^{i\varphi} |-\rangle), \tag{1}$$

where $E_0(x, y)$ is the amplitude, and $|+\rangle = (\hat{x} + i\hat{y})/\sqrt{2}$ and $|-\rangle = (\hat{x} - i\hat{y})/\sqrt{2}$ represent the right and left circular polarization states, respectively [29, 41].

We first consider a homogeneous uniaxial slab with a birefringent phase retardation of π. In the principal axes reference frame the Jones matrix for this half-wave plate (HWP) is $T_0 = \text{diag}[1, -1]$. If the optical axis is rotated an angle α about the z axis, the transmission matrix will become $T = R(-\alpha)T_0R(\alpha)$, where $R(\alpha)$ is the usual rotation matrix for a rotation by α in the xy plane [20, 34]. That is,

$$T = \begin{pmatrix} \cos 2\alpha & \sin 2\alpha \\ \sin 2\alpha & -\cos 2\alpha \end{pmatrix}. \tag{2}$$

Let us now examine the more general situation in which the orientation of the optical axis varies with position. Specifically, the optical axis in the xy plane is assumed to be

$$\alpha = q\theta + \alpha_0, \tag{3}$$

where q and α_0 are constants and $\theta = \arctan(y/x)$ is the azimuthal angle [20, 42, 43]. The topological charge q represents the number of rotations of the local optical axis around the center of the slab. This slab, known as q-plate [20], is one type of inhomogeneous wave plate that can be used for unique applications, e.g. generating vortex or vector beams. It can be implemented by diverse materials, such as subwavelength diffraction gratings [18, 19], liquid crystals [20, 27, 28, 30, 32, 33], segmented birefringent crystals [22, 23, 44], and metasurfaces [25, 26].

Immediately following interaction with the q-plate, the light distribution becomes $\mathbf{E}(x, y, 0) = T\mathbf{E}_i(x, y, 0)$. Using Eqs. (1) and (2) the exiting light can be written as

$$\mathbf{E}(x, y, 0) = E_0[\sin \vartheta e^{-i(2\alpha - \varphi)} |+\rangle + \cos \vartheta e^{i(2\alpha - \varphi)} |-\rangle]. \tag{4}$$

Comparison of Eqs. (1) and (4) shows that the initial left (right) circular polarization component is converted into the exiting right (left) circular polarization one completely, simultaneously obtaining a PB phase [45, 46] of -2α (2α).

Note that Eq. (4) can also be regarded as the polarization state $\mathbf{E}(x, y, z)$ at positions $z \neq 0$ if the incident light is assumed to be a plane wave. This is a simplified model commonly adopted in the literature, especially to analyze the polarization of a vector beam [25–30]. However, it can not account for the propagation behavior of the beam. In the following, we analyze the practical propagation of a light beam diffracted by a q-plate.

2.1. Vector beam in the Fresnel diffraction region

We implement the q-plate with dielectric metasurfaces. Acting as a pure phase element, the ultra-thin metasurface imprints a PB phase on the incident light. At the same time, it is an inhomogeneous anisotropic plate. Therefore, the vector field beyond the metasurface can be worked out through vector diffraction calculations [37, 38]. Following this method, the outgoing light at a position z can be derived in the paraxial approximation by using the Fresnel diffraction integral

$$\mathbf{E}(x, y, z) = \frac{\exp(ikz)}{i\lambda z} \int_{-\infty}^{\infty} \int_{-\infty}^{\infty} dx' dy' \mathbf{E}(x', y', 0) \exp\left\{i\frac{k}{2z}[(x - x')^2 + (y - y')^2]\right\}. \quad (5)$$

For simplicity we assume an incident Gaussian beam $E_0(x, y) = \exp\left[-(x^2 + y^2)/w_0^2\right]$, where w_0 is the beam waist. The results for other types of incident beams can be derived similarly.

We substitute Eq. (4) into Eq. (5) and denote

$$\mathbf{E}(x, y, z) = E_+|+\rangle + E_-|-\rangle. \quad (6)$$

By taking advantage of the inherent circular symmetry of the source field and the phase plate, the circular polarization components can be worked out in the cylindrical coordinate system using $x' = \rho \cos \phi$, $y' = \rho \sin \phi$, $x = r \cos \theta$, and $y = r \sin \theta$:

$$E_\pm = c_\pm \frac{\exp[ik(z + \frac{r^2}{2z}) \pm i\varphi]}{i\lambda z} \int_0^\infty \int_0^{2\pi} \rho d\rho d\phi E_0 \exp\left[ik\frac{\rho^2}{2z} - i\frac{kr\rho}{z} \cos(\phi - \theta) \mp i2\alpha\right], \quad (7)$$

where $c_+ = \sin \vartheta$, $c_- = \cos \vartheta$. Using the Jacobi-Anger expansion $\exp(iu\cos\psi) = \sum_{m=-\infty}^{\infty} i^m J_m(u) \exp(-im\psi)$ and $J_m(-u) = J_{-m}(u) = (-1)^m J_m(u)$, the integration over ϕ can be carried out, leading to

$$E_\pm = c_\pm \frac{\exp[ik(z + \frac{r^2}{2z}) \mp i(2\alpha - \varphi)]}{i\lambda z} 2\pi(-1)^{|q|} \int_0^\infty \exp\left(-\frac{\rho^2}{w_0^2} + ik\frac{\rho^2}{2z}\right) J_{2|q|}\left(\frac{kr\rho}{z}\right) \rho d\rho. \quad (8)$$

By using the reference expression [47]

$$\int_0^\infty x^\mu e^{-\alpha x^2} J_\nu(\beta x) dx = \frac{\beta^\nu \Gamma(\frac{\mu+\nu+1}{2})}{2^{\nu+1}\alpha^{\frac{\mu+\nu+1}{2}}\Gamma(\nu+1)} {}_1F_1\left(\frac{\mu+\nu+1}{2}, \nu+1, -\frac{\beta^2}{4\alpha}\right), \quad (9)$$

the above integral can be evaluated to give

$$E_\pm = c_\pm A(r, z) e^{ikz + ik\frac{r^2}{2z} \mp i(2\alpha - \varphi)}. \quad (10)$$

Here ${}_1F_1$ is the Kummer confluent hypergeometric function and

$$A(r, z) = \frac{2^{-2|q|}\sqrt{\pi}}{\Gamma(1/2 + |q|)} \frac{kw_0^2}{kw_0^2 + i2z} \left(\frac{-ik^2r^2w_0^2}{2kw_0^2z + i4z^2}\right)^{|q|} {}_1F_1\left(1 + |q|, 1 + 2|q|, -\frac{ik^2r^2w_0^2}{2kw_0^2z + i4z^2}\right). \quad (11)$$

To gain more insight into the result, we use the formula $_1F_1(a, b, -z) = \exp(-z)_1F_1(b - a, b, z)$ [47] to rewrite Eq. (10) as

$$E_\pm = c_\pm G(r, z)e^{\mp i(2\alpha-\varphi)} \left(\frac{-ik^2r^2w_0^2}{2kw_0^2z + i4z^2}\right)^{|q|} \frac{2^{-2|q|}\sqrt{\pi}}{\Gamma(1/2 + |q|)} {}_1F_1\left(|q|, 1 + 2|q|, \frac{ik^2r^2w_0^2}{2kw_0^2z + i4z^2}\right), \quad (12)$$

where $G(r, z)$ represents the common Gaussian beam

$$G(r, z) = \frac{kw_0^2}{kw_0^2 + i2z} e^{ikz - \frac{kr^2}{kw_0^2 + i2z}}. \quad (13)$$

Eq. (12) indicates that the action of the q-plate is to introduce a vortex phase and a modification of a confluent hypergeometric function onto the underlying Gaussian beam.

Using Eqs. (6) and (10) the analytical expression for vector beam can be obtained. In the following we give the results for three classes of vector beams of which the polarization states cover the higher-order Poincaré sphere [2, 3].

Elliptically polarized vector beam. Inserting Eq. (10) into Eq. (6), we obtain a general expression for the exit beam leaving the q-plate

$$\mathbf{E}(x, y, z) = A(r, z)e^{ikz + ik\frac{r^2}{2z}} [\sin\vartheta e^{-i(2\alpha-\varphi)}|+\rangle + \cos\vartheta e^{i(2\alpha-\varphi)}|-\rangle]. \quad (14)$$

It clearly shows that the outgoing beam exhibits a distribution determined by a hypergeometric function. When $q = 0$ Eq. (14) reduces to the common Gaussian beam expression. Furthermore, the x and y field components can be obtained by substituting Eq. (10) into $E_x = (E_+ + E_-)/\sqrt{2}$ and $E_y = i(E_+ - E_-)/\sqrt{2}$, yielding

$$\mathbf{E}(x, y, z) = \frac{1}{\sqrt{2}} A(r, z)e^{ikz + ik\frac{r^2}{2z}} \begin{bmatrix} \sin\vartheta e^{-i(2\alpha-\varphi)} + \cos\vartheta e^{i(2\alpha-\varphi)} \\ i\sin\vartheta e^{-i(2\alpha-\varphi)} - i\cos\vartheta e^{i(2\alpha-\varphi)} \end{bmatrix}. \quad (15)$$

It is worthy of pointing out that: (i) The polarization in Eq. (14) represents a state on the higher-order Poincaré sphere [2, 3]. As demonstrated in [29], any polarization evolution on the higher-order Poincaré sphere can be realized by changing the incident polarization and the q-plate. Therefore, Eq. (14) can represent any vector beam on the higher-order Poincaré sphere produced by a metasurface. (ii) If the incident wave is a plane wave, that is, E_0 is a constant in Eq. (4), then one can follow the above analysis to show that the resultant wave has the same polarization as that of the incident Gaussian beam, i.e. Eq. (14). This is the reason that it is safe to replace a light beam by a plane wave to simplify analysis on vector beams generated by q-plates in the literature [19–31]. (iii) Comparing Eqs. (14) and (4), one can find that the light beam preserves its polarization during propagation. This holds true only for the case of the q-plate having a retardation of π, for which there is a complete conversion between the two circular polarization components. For a general metasurface with arbitrary retardation, partial cross-polarization conversion may occur. Consequently the converted light interferes with the residual beam and thus the generated vector beam has a hybrid polarization that may change during propagation like a full Poincaré beam [14]. This vector beam may also lead to an azimuthal spin splitting [36, 48, 49], namely the azimuthal spin Hall effect of light [50, 51].

Note that scalar vortex beams in the form of a hypergeometric function produced by use of computer-generated holograms or of spiral phase plates have been discussed as early as in [52] and later in [53–55], and are called Kummer or hypergeometric beams [56–58]. In comparison, the vector beam generated by a q-plate has a similar hypergeometric function form. This is reasonable since the vector beam can be regarded as a combination of two circularly polarized vortices evident in Eq. (14). But the vector beam possesses spatially varying

polarization which leads to strikingly different properties of beam. For example, in contrast to the scalar vortex beams which have a homogeneous polarization distribution, vector beams have an inhomogeneous transverse polarization and a strong longitudinal field when tightly focused. It is due to this type of polarization structure that vector beams have unique properties [1] and find a variety of applications [4–12]. Moreover, following the above conclusion (iii), a vector beam generated by a general metasurface with a retardation other than π will have a form completely different from that of scalar vortex beams [25, 36], thus exhibiting different propagation behavior [14, 49].

Linearly polarized vector beams. If the incident light is linearly polarized ($2\vartheta = \pi/2$, i.e., along the equator of the Poincaré sphere), then the emerging light is an azimuthal-variant linear polarization,

$$\mathbf{E}(x, y, z) = A(r, z)e^{ikz + ik\frac{r^2}{2z}} \begin{bmatrix} \cos(2\alpha - \varphi) \\ \sin(2\alpha - \varphi) \end{bmatrix}. \tag{16}$$

Circularly polarized vortex beam. If the incident light is a circular polarization $|\pm\rangle$, the exit light is an opposite circular polarization vortex,

$$\mathbf{E}(x, y, z) = A(r, z)e^{ikz + ik\frac{r^2}{2z} \mp i(2\alpha - \varphi)}|\mp\rangle. \tag{17}$$

As such, the spin angular momentum of the incident beam is converted into the orbital angular momentum of the exit beam. This is the case discussed previously in [20, 34, 35].

2.2. Vector beam in the Fraunhofer diffraction zone

It is well known that the result of Fraunhofer diffraction is an approximation of Fresnel diffraction that only considers contributions from incident wave components with planar wavefronts [37, 39]. That is to say, the vector beam in the Fraunhofer diffraction region can be obtained by omitting terms containing x'^2 and y'^2 in Eq. (5) or those related with ρ^2 in Eq. (8). Following similar steps in the above subsection, the vector beam can be obtained. We find that the vector beam has the same form as those above with the exception that:

$$A(r, z) = \frac{2^{-2|q|}\sqrt{\pi}}{\Gamma(1/2 + |q|)} \frac{kw_0^2}{2iz} \left(-\frac{k^2 r^2 w_0^2}{4z^2}\right)^{|q|} {}_1F_1\left(1 + |q|, 1 + 2|q|, -\frac{k^2 r^2 w_0^2}{4z^2}\right). \tag{18}$$

This result can also be obtained by applying the condition $z \gg kw_0^2/2$ to Eq. (11).

3. Experimental verifications

To verify the theory, we built an experimental setup as shown in Fig. 1(a). A He-Ne laser produces a fundamental Gaussian beam that was then collimated and expanded with a waist $w_0 = 1.75$ mm. Next the beam was appropriately polarized by orienting a polarizer (GLP1) and a quarter-wave plate (QWP1) in its path before being sent through the metasurface. For quantitative study we designed three typical metasurfaces with $q = 0.5, 1$, and 1.5. They were fabricated by etching continuously varying grooves in a fused silica sample using a femtosecond laser [25, 26]. The resulting self-assembled nanogratings behave effectively as an inhomogeneous HWP. Another quarter-wave plate (QWP2) and a polarizer (GLP2) were added to measure the Stokes parameters of the resulting beam. The intensity of the output vector beam was recorded by a CCD.

3.1. Results for Fresnel diffraction

Let the position of the metasurface be denoted as $z = 0$. We illuminated the metasurface with an x-polarized Gaussian beam to generate linearly polarized vector beams. The theoretical output
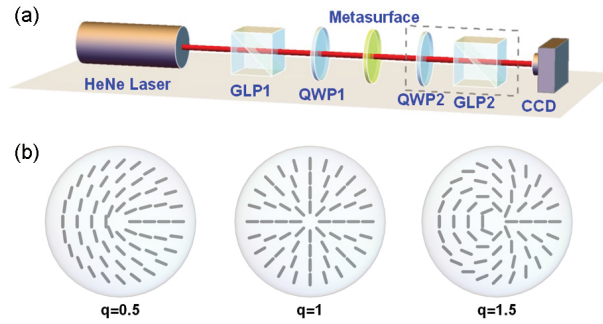
Fig. 1. (a) Experimental setup to generate vector beams. A He-Ne laser (632.8 nm, 17 mW, Thorlabs HNL210L-EC) outputs a linearly polarized Gaussian beam. GLP, Glan laser polarizer; QWP, quarter-wave plate; CCD, charge coupled device (Coherent LaserCam HR). (b) Schematic illustrations of the orientation of local optical axes in three pieces of metasurfaces used in the experiments.
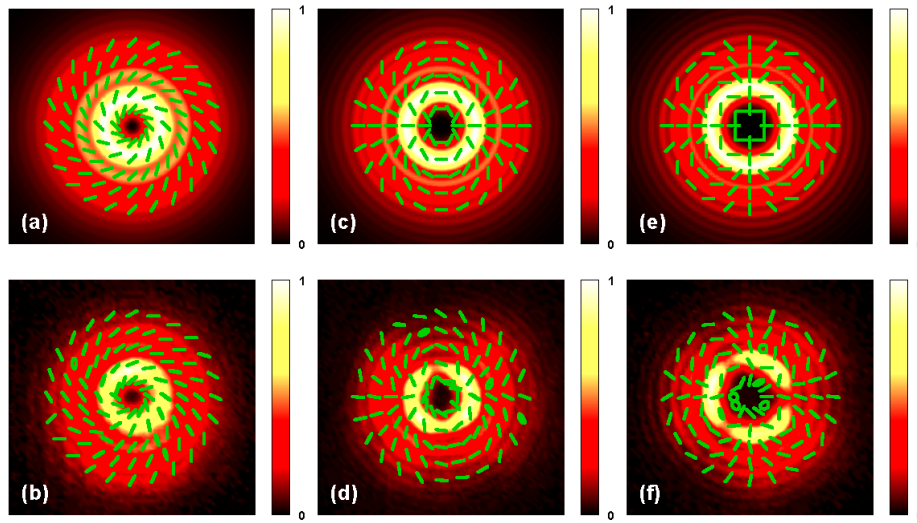

Fig. 2. Normalized transverse intensities and local polarization distributions of vector beams generated with metasurfaces of different topological charge q. The left, middle and right columns correspond to $q = 0.5$, 1 and 1.5, respectively. The top and bottom rows are theoretical and experimental results, respectively.

Fig. 3. The radial intensity distributions for vector beams generated with metasurfaces of different topological charge q. (a) and (b) are theoretical and experimental results measured at $z = 50$ cm, respectively.
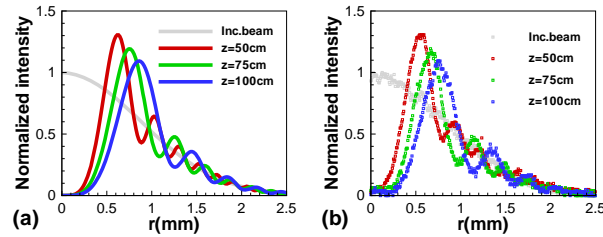

Fig. 4. The radial intensity distributions for vector beam measured at different propagation distances. (a) and (b) are theoretical and experimental results for the case $q = 1$, respectively. The intensities are normalized by the center intensity of the incident Gaussian beam.

intensities calculated by Eq. (16) and the experimental results measured at $z = 50$ cm are shown in Fig. 2. It is seen that the transverse intensity consists of a sequence of concentric rings. In the spirit of the geometrical theory of diffraction [59], this result may be regarded as the sum of two contributions: The first is from the geometrically propagating wave carrying the geometrical phase; The second is from the diverging wave diffracted from the singularity. The interference of the two contributions then leads to a ringing effect, i.e. the oscillation of the radial intensity magnitude, as shown in Figs. 2-4. From this description, one may find methods to remove such ringing effects. For example, one can adopt a hollow incident beam, e.g. hollow Gaussian beams [60], to avoid the diffraction at the central singularity completely. Also, one can convert the diverging wavefront diffracted from the singularity into a planar one, e.g. by using a spherical lens, so as to obtain a single-ring vector beam. This method will be investigated experimentally in Sec.3.2.

To study the relation of the intensity of the vector beam to the q value, we plotted the intensity in Fig. 2 along one line as a function of distance from the center. The results are shown in Fig. 3, where the experimental results agree remarkably well with the theoretical ones. One can see that the radii of the light rings of the vector beams increase as the q value increases.

At the same time, we investigated the dependence of the intensity on the propagation distance z. As an example, we chose a $q = 1$ metasurface and measured the intensity at $z = 50, 75,$ and 100 cm. The results are plotted in Fig. 4, showing that the radius and width of the inner ring of the vector beam increases with z, while the magnitude decreases over the course of propagation.

In addition, a polarizer was inserted before the CCD, and the intensity was then measured to help analyze the polarization state. When the polarizer is along the 0°, 45°, 90°, and 135° directions relative to the x axis, the results corresponding to the beams in Figs. 2(c) and 2(d) are illustrated in Fig. 5. One can see that the polarized intensities are petal-shaped, with the number of petals being equal to $4q$. Interestingly, the intensity patterns rotate at a angular velocity half
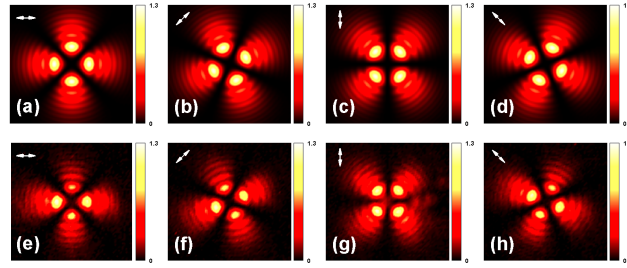
Fig. 5. The intensity distributions of a vector beam passing through a linear polarizer. The transmission axis of the polarizer is indicated by the arrow at the upper left corner. The top and bottom rows are theoretical and experimental results, respectively. Here $q = 1$ and $z = 50$ cm.
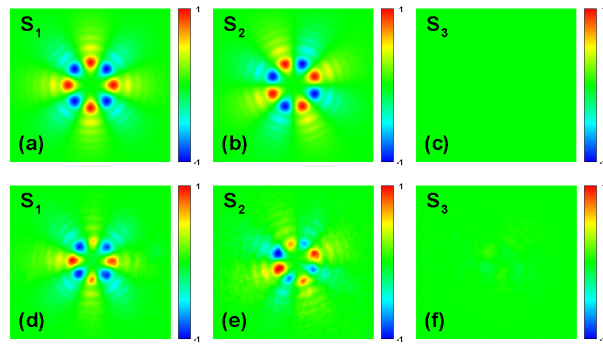

Fig. 6. Stokes parameters for the case $q = 1$ and $z = 50$ cm. The top and bottom rows are respectively theoretical and experimental results, corresponding to Figs. 2(c) and 2(d).

of that of the polarizer, which is consistent with the theory. The excellent agreement between the theoretical and experimental results in Fig. 5 indicates the beam in Fig. 2(d) has a polarization distribution as that in Fig. 2(c).

Further, the Stokes parameters were measured to analyze the vector polarization. The Stokes parameters are S_0, simply the intensity of the output beam, $S_1 = I(0°, 0°) - I(90°, 90°)$, $S_2 = I(45°, 45°) - I(135°, 135°)$, and $S_3 = I(-45°, 0°) - I(45°, 0°)$. Here $I(\alpha, \beta)$ is the intensity recorded by the CCD when the optical axis of QWP2 and the polarization direction of GLP2 stay with α and β against the x axis, respectively. As an example, the measured results and those calculated by Eq. (16) for $q = 1$ and $z = 50$ cm are presented in Fig. 6. The Stokes parameters were employed to retrieve the polarization state [29, 41] according to the relationship [39, 40]:

$$S_1 = S_0 \sin 2\vartheta \cos 2\varphi, \quad S_2 = S_0 \sin 2\vartheta \sin 2\varphi, \quad S_3 = S_0 \cos 2\vartheta. \tag{19}$$

The retrieved results for $q = 0.5, 1$, and 1.5 are plotted in Fig. 2. The overall tendency of the azimuthal change in vector polarization in the experimental results is in accordance with the theoretical results. We note that the differences, including the appearance of polarization ellipses, may result from either experimental or calculation errors.

In the above, the properties of linearly polarized vector beams are investigated. We also studied an elliptically polarized vector beam and a circularly polarized vortex beam, formed via incidence of elliptical and circular polarizations (by controlling GLP1 and QWP1 in Fig. 1(a) [29]), respectively (not shown here). It is found that the intensity distributions for the latter two cases are the same as that of the former. This indicates that the intensity of vector beams
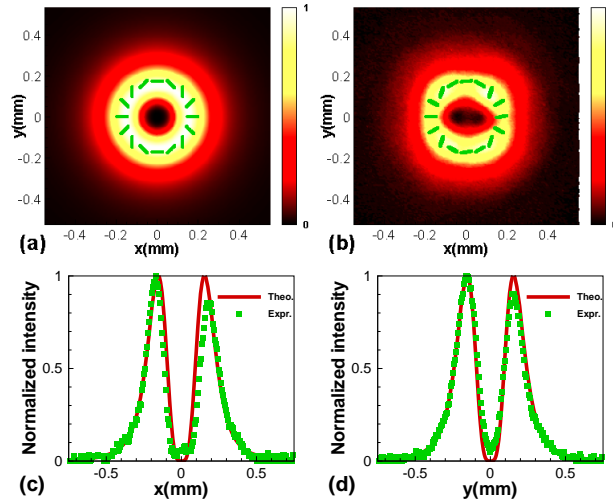
Fig. 7. Distributions of normalized intensity and polarization of vector beam for the case $q = 1$ in the Fraunhofer region ($f = 100$ cm). (a) and (b) are theoretical and experimental results, respectively. (c) and (d) are intensities on the x and y axes.

generated by half-wave metasurfaces is independent of their specific polarization.

3.2. Results for Fraunhofer diffraction

Theoretically, Fraunhofer diffraction naturally appears when propagation distance $z >> k\rho^2/2$. For the parameters $w_0 = 1.75$ mm and $\lambda = 632.8$ nm, $z >> 95$ m is necessary, which is difficult to achieve in the laboratory. Alternatively, a thin optical lens [37] can be inserted immediately behind the metasurface. If the CCD is placed at the focus of the lens ($z = f$), the phase factor $\exp(-ik\rho^2/2f)$ produced by the lens exactly cancels out $\exp(ik\rho^2/2z)$ in Eq. (5), leading the field measured by the CCD to be the same result as the Fraunhofer diffraction region.

Here we choose a thin lens with the focal length $f = 100$ cm. The theoretical result calculated by Eqs. (16) and (18) and the experimental result are shown in Fig. 7. One can see that the vector beam displays a perfect single ring, distinct from the multi-ringed structure in the case of Fresnel diffraction. This result verifies the second method proposed in Sec.3.1 to remove the ringing effect. Consequently, we obtain a pure vector beam, with all the energy on a single ring.

To verify the theory, the intensities along the x and y axes in Figs. 7(a) and 7(b) were plotted for comparison in Figs. 7(c) and 7(d). The excellent agreement between the theoretical and experimental results proves that the theory of Eqs. (16) with (18) is correct. In addition, one can show that there is not essential difference between these intensities and the common model of vector beam, i.e. Laguerre-Gaussian beam (not shown here). Therefore, Fraunhofer diffraction provides a method to remove the multi-ringed effect in Fresnel diffraction and the resultant single ring can be an ideal model of the vector beams investigated in the literature.

Next the intensity of the vector beam passing through a polarizer was used to qualitatively analyze the polarization state. The calculated and measured results are shown in Fig. 8. It shows that the theory agrees very well with the experiment. The rotational characteristics of the petal-shaped intensity in Fig. 8 are consistent with the polarization distribution of Fig. 7(a), thereby validating the experimental polarization result in Fig. 7(b). In addition, the petal-shaped intensity distribution in Fig. 8 is clean, without diffraction fringes as in Fig. 5. This fact shows again the advantage of Fraunhofer diffraction in achieving pure vector beams.

Finally, the Stokes parameters were measured to discover the polarization state. The results
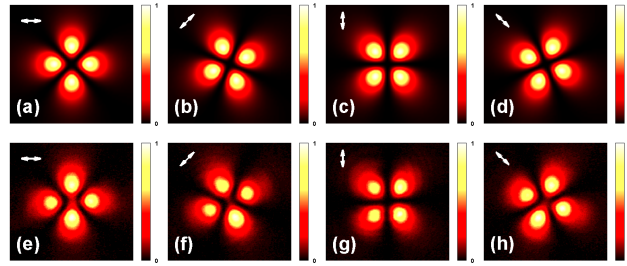
Fig. 8. The intensity distributions of the resultant vector beam passing through a linear polarizer for the case $q = 1$ in the Fraunhofer region ($f = 100$ cm). Transmission axis of the polarizer is indicated by an arrow at the upper left corner. The top and bottom rows are theoretical and experimental results, respectively.
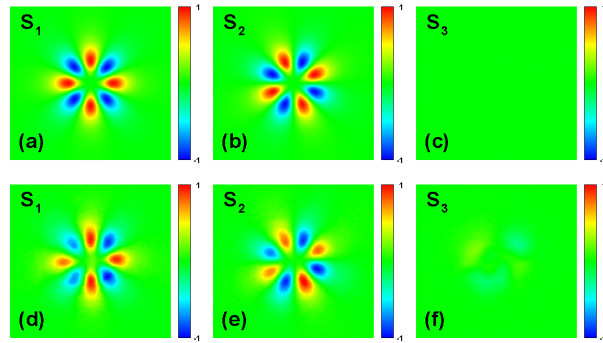

Fig. 9. Stokes parameters for the case $q = 1$ in the Fraunhofer region ($f = 100$ cm). The top and bottom rows are respectively theoretical and experimental results corresponding to Fig. 7(a) and 7(b).

calculated using Eqs. (16) and (18) and those measured are presented in Fig. 9. Then the Stokes parameters were used to retrieve the polarization state according to the relation Eq. (19). The theoretical and experimental results are respectively illustrated in Figs. 7(a) and 7(b), revealing an excellent agreement.

4. Conclusion

In conclusion, we have proposed a propagation model for vector beams produced by dielectric metasurfaces. Using vector diffraction theory, analytical forms for vector beams produced beyond metasurfaces with arbitrary incident polarization were found in the Fresnel and Fraunhofer diffraction regions. The vector beam has a complex amplitude proportional to a confluent hypergeometric function. The intensity profile produces concentric rings in the Fresnel region, but in the Fraunhofer region is a single ring containing all of the outgoing energy. Therefore, Fraunhofer diffraction can provide an efficient way to obtain vector beams with simultaneously high purity and modal power. All the theoretical results have been verified by experiments satisfactorily.

These results can be applied in the study of optical phenomena involving PB phase in metasurfaces. Any vector fields on the higher-order Poincaré sphere [2, 3] generated by metasurfaces [29] can be expressed, and their properties can be investigated by using the above results. Other applications include the conversion between spin and orbital angular momenta [20, 34, 35] and the azimuthal spin splitting [48–50], i.e. the azimuthal spin Hall effect of

light [51], in q-plates. In addition, only metasurfaces with a birefringent phase retardation of π are considered in the present paper. If other metasurfaces are used, additional new properties of vector beams can be found. For example, a vector beam may not continue to preserve its polarization structure upon propagation, leading to interesting phenomena similar to the full Poincaré beam [14]. Study of these issues will be left to future work.

Funding